AIP | Journal of Applied Physics

Magnetization-steps in Y2CoMnO6 double perovskite: The role of antisite disorder

Harikrishnan S. Nair, R. Pradheesh, Yinguo Xiao, Dona Cherian, Suja Elizabeth, Thomas Hansen, Tapan Chatterji, and Th. Brückel

Citation: Journal of Applied Physics **116**, 123907 (2014); doi: 10.1063/1.4896399
View online: http://dx.doi.org/10.1063/1.4896399
View Table of Contents: http://scitation.aip.org/content/aip/journal/jap/116/12?ver=pdfcov
Published by the AIP Publishing

Magnetization-steps in Y_2CoMnO_6 double perovskite: The role of antisite disorder

Harikrishnan S. Nair,[1,a)] R. Pradheesh,[2] Yinguo Xiao,[1] Dona Cherian,[3] Suja Elizabeth,[3] Thomas Hansen,[4] Tapan Chatterji,[4] and Th. Brückel[1]
[1]*Jülich Center for Neutron Sciences-2/Peter Grünberg Institute-4, Forschungszentrum Jülich GmbH, 52425 Jülich, Germany*
[2]*Low Temperature Physics Laboratory, Department of Physics, Indian Institute of Technology Madras, Chennai 600036, India*
[3]*Department of Physics, Indian Institute of Science, C. V. Raman Avenue, Bangalore 560012, India*
[4]*Institut Laue-Langevin, BP 156, 38042 Grenoble Cedex 9, France*

(Received 1 August 2014; accepted 12 September 2014; published online 24 September 2014)

Antisite disorder is observed to have significant impact on the magnetic properties of the double perovskite Y_2CoMnO_6 which has been recently identified as a multiferroic. A paramagnetic-ferromagnetic phase transition occurs in this material at $T_c \approx 75$ K. At 2 K, it displays a strong ferromagnetic hysteresis with a significant coercive field of $H_c \approx 15$ kOe. Sharp *steps* are observed in the hysteresis curves recorded below 8 K. In the temperature range $2\,K \leq T \leq 5\,K$, the hysteresis loops are anomalous as the virgin curve lies outside the main loop. The field-cooling conditions as well as the rate of field-sweep are found to influence the *steps*. Quantitative analysis of the neutron diffraction data shows that at room temperature, Y_2CoMnO_6 consists of 62% of monoclinic $P2_1/n$ with nearly 70% *antisite* disorder and 38% *Pnma*. The bond valence sums indicate the presence of other valence states for Co and Mn which arise from disorder. We explain the origin of *steps* by using a model for pinning of magnetization at the antiphase boundaries created by *antisite* disorder. The *steps* in magnetization closely resemble the martensitic transformations found in intermetallics and display first-order characteristics as revealed in the Arrott's plots. © *2014 AIP Publishing LLC*. [http://dx.doi.org/10.1063/1.4896399]

I. INTRODUCTION

The crystallographically "ordered" rare earth double perovskite oxides, $R_2MM'O_6$ (R = rare earth; M/M' = transition metal), are ferromagnetic insulators possessing high magnetic transition temperatures near or above room temperature (RT). Being ferromagnetic insulators, they are prospective materials for spin polarization and spintronics applications. In addition, they display room-temperature magnetocapacitance[1] and show potential for multiferroicity.[2–7] The multiferroic nature has been predicted theoretically through dielectric anomalies and polar behaviour in double perovskites. First-principles density functional calculations have shown the existence of soft phonons which modify the superexchange interaction between Ni and Mn in La_2NiMnO_6.[8] Introducing size-disorder through substituting La with Lu is predicted to result in polar behaviour in the same compound.[2] In another work, it was found that the normal insulating state of La_2CoMnO_6, which is driven by the electron correlations and spin-orbital coupling, is driven to half-metallicity through the introduction of external pressure.[9] This is achieved through spin-state transitions of the Co ion. These studies make it clear that the structural, electronic, and magnetic properties of double perovskites can be altered through the tuning of cationic size, external or chemical pressure, and valence states of the transition metal.

Ferromagnetism in the double perovskites is explained in terms of Goodenough-Kanamori rules[10,11] operating through the exchange paths M^{2+}-O-M'^{4+}. It assumes perfect crystallographic order of the M^{2+} and M'^{4+} cations in the $2c$ ($0\ \frac{1}{2}\ 0$) and $2d$ ($\frac{1}{2}\ 0\ 0$) Wyckoff positions. However, perfect order is seldom achieved in real samples. The samples prepared in a laboratory have *antisite* disorder where the transition metal cations occupy the positions $2c$ and $2d$ interchangeably. This disorder introduces M-O-M and M'-O-M' exchange paths and consequently affects the perfect ferromagnetism of the otherwise ordered lattice by creating antiferromagnetic clustered regions. This leads to reduction in T_c and saturation magnetization.[12] The effects of disorder on the magnetic behaviour of double perovskites have been carefully studied in La_2CoMnO_6 and La_2NiMnO_6.[13,14] For example, a multi-phase domain structure with two distinguishable ferromagnetic regions has been observed in La_2CoMnO_6.[13] The nearly ordered ferromagnetic phase displayed a $T_c \approx 226$ K while the second phase had $T_c < 150$ K. Local atomic disorder and formation of antiphase domains were observed in La_2NiMnO_6.[14] It was found that prolonged annealing procedures did not remove the antiphase domain boundaries. The antisite disorder and the antiphase boundaries have been experimentally observed using Mössbauer spectroscopy, transmission electron microscopy, and Lorentz transmission electron microscopy.[15–17] It is now understood how the magnetic domain walls are pinned to the antiphase boundaries and how the application of magnetic field changes the magnetic domain structure.[17]

a)krishnair1@gmail.com

A careful study of the magnetism of rare earth double perovskites incorporating the disorder effects and the anti-phase domains assumes importance especially after the observation of multiferroicity in Lu_2MnCoO_6[4] and in Y_2CoMnO_6.[5] In the present article, we report the results of experimental investigation on the double perovskite Y_2CoMnO_6 using magnetization, specific heat, and neutron diffraction by taking into account the role of *antisite* disorder. Sharp *steps* in magnetic hysteresis below 8 K are observed in this compound which can be related to the *antisite* disorder. Field-induced *steps* in magnetization have been observed in several classes of materials like the geometrically frustrated magnets,[18] magnetic cluster materials,[19] spin chain compounds,[20] intermetallics,[21,22] and in manganites.[23] In the case of intermetallics, as the applied magnetic field is varied the elastic strain at the domain boundaries acts against the antiferromagnetic–ferromagnetic transformation and leads to the *steps* in magnetization. The role of disorder in the occurrence of sharp steps in magnetic hysteresis has been studied in detail in the case of $CeFe_2$.[24,25] Martensitic scenario[25] and disorder-influenced first-order nature of the magnetization steps[24] have been confirmed in the case of $CeFe_2$-based intermetallics. We argue that a very similar role is played by *antisite* disorder in the case of Y_2CoMnO_6.

II. EXPERIMENTAL DETAILS

Polycrystalline samples of Y_2CoMnO_6 were prepared through standard ceramic routes using high purity Y_2O_3, Co_3O_4, and MnO_2 as starting materials. The precursors were mixed together in stoichiometric ratios and ground in a mortar and pestle before heating the mixture up to 1320 °C in a furnace for 48 h. The procedure of grinding and heating was repeated until a single phase was formed. X ray diffraction of the synthesized powder was carried out using a Huber diffractometer G670 (Cu-Kα) to determine the phase and to rule out the presence of major impurities. Magnetic measurements in zero field-cooled (ZFC) and field-cooled (FC) cycles were performed in a commercial Magnetic Property Measurement System which uses a 7 T superconducting magnet and also using the vibrating sample magnetometer option in a Physical Property Measurement System (both Quantum Design, Inc.) with a 9 T magnet. Low temperature x ray diffraction patterns recorded for Y_2CoMnO_6 did not give evidence for any structural phase transitions down till 10 K. Initial structural refinements using the x ray data were performed using monoclinic $P2_1/n$ and *Pnma* space groups;[13] however, it was not possible to distinguish between these space groups as both the models gave equally good fits.[26] *Antisite* disorder is an important effect in these materials and a quantitative estimate of the disorder has to be obtained to correlate with the magnetic properties. Since the neutron scattering lengths are quite different for Co and Mn (b_{coh} (Co) = 2.49 fm, b_{coh} (Mn) = −3.75 fm),[27] neutrons are the ideal probe for studying the disorder effects in these compounds. Neutron powder diffraction experiments on approximately 10 g powder were carried out on the instrument D20 at ILL, Grenoble, employing a wavelength, $\lambda = 1.87$ Å. Structural and magnetic refinements were performed using the Rietveld method[28] coded in the FullProf suite of programs.[29] The software SARA*h*[30] was used for the magnetic structure determination procedure using representational analysis.

III. RESULTS AND DISCUSSION

A. Magnetization

The magnetization profiles $M(T)$ of Y_2CoMnO_6 in ZFC and FC cycles at different applied magnetic fields are presented in Figure 1. A magnetic phase transition is evident at $T_c \approx 75$ K. Below T_c, the field cooled magnetization increases and eventually reaches a value close to 3 μ_B/f.u. at an applied magnetic field of 50 kOe. Through Curie-Weiss (CW) analysis, an effective paramagnetic moment value of $\mu_{eff} = 6.2(3)$ μ_B/f.u. and Curie-Weiss temperature, $\Theta_{CW} = 70(2)$ K are estimated, implying predominant ferromagnetic exchange in the material as predicted by the Goodenough-Kanamori rules.[10,11] The magnetization data for $T > 150$ K ($\approx 2T_c$) was used for the CW analysis.

As a comparison, the ordered sample of La_2CoMnO_6 showed an effective paramagnetic moment of 7.83 μ_B/f.u. compared to the disordered samples which showed a reduction in the value to 6.63 μ_B/f.u.[12] This reduction in magnetic moment is much clearly visible in the magnetic hysteresis plots at low temperatures (presented later) where a saturation magnetization of only 3.5 μ_B/f.u. is attained. A perfectly ordered lattice of Mn/Co should give rise to 6 μ_B/f.u.[12] The maximum magnetization obtained for our samples is lower than the value obtained for La_2CoMnO_6[12] which indicated greater degree of disorder in our samples. The reduction in magnetic moment compared to that of the perfectly ordered samples is normally attributed to the formation of Co^{2+}-O-Co^{2+} and Mn^{4+}-O-Mn^{4+} antiferromagnetic bonds. In the subsequent sections where we analyze the neutron diffraction data, we show that this is indeed the case in Y_2CoMnO_6 where *antisite* disorder leads to the formation of different valences of Co and Mn and thereby reduce the perfect ferromagnetism.

B. "Steps" in magnetic hysteresis

The magnetic hysteresis of Y_2CoMnO_6 at 2 K presented in Figure 2(a), displays a prominent ferromagnetic loop.

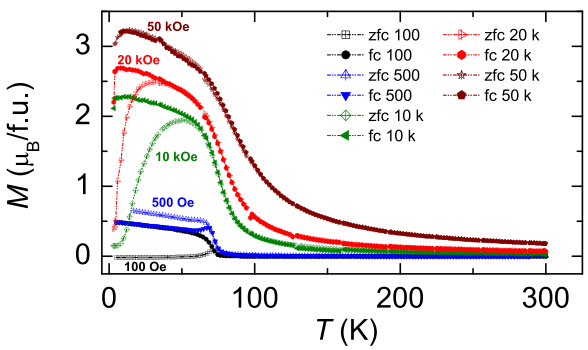

FIG. 1. Magnetization curves of Y_2CoMnO_6 in ZFC (open symbols) and FC (closed symbols) cycles at different applied fields. A magnetic phase transition at 75 K is clear from the low-field data. As the applied field >10 kOe, the curves show a downturn at low temperatures.

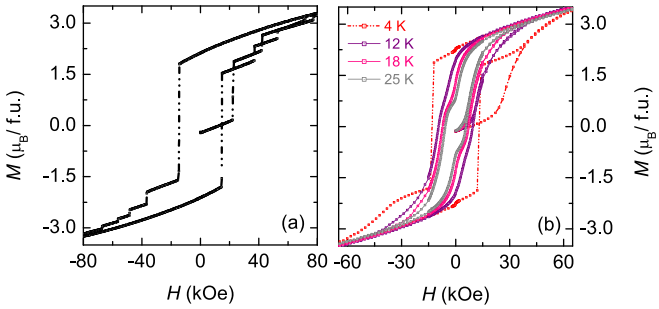

FIG. 2. (a) Sharp *steps* in the magnetic hysteresis of Y_2CoMnO_6 at 2 K. The *steps* are observed only in the forward field-sweep direction. The virgin loop is found to lie outside the rest of the envelope. (b) The hysteresis plots in the temperature range 4 K to 25 K. The *steps* vanish above 8 K.

Several peculiar features are noticeable, *viz.*, (i) the *virgin curve* lies outside the envelope of further magnetization cycles and displays sharp *steps* in magnetization; (ii) in the reverse-sweep of the magnetic field, i.e., for H: 9 kOe $\rightarrow$ 0 kOe, the *steps* are absent; (iii) in the subsequent negative field-cycle (H: 0 kOe $\rightarrow$ −9 kOe), they re-appear. At 2 K, the hysteresis curve presents a coercive field of $H_c \sim 14.6(2)$ kOe and remnant magnetization of 2.12(4) μ_B/f.u. As the temperature is increased beyond 8 K, the *steps* in magnetization are reduced in magnitude and number and eventually they disappear. This is clear from Figure 2(b).

In order to understand the nature of the *steps* in the hysteresis curves, different field-cooling conditions and sweep rates were administered to measure magnetization. The hysteresis curves at 2 K measured under two applied fields, $H_1 = 10$ and $H_2 = 25$ kOe, are shown in Figure 3. The values of applied field $H_2 \sim 25$ kOe corresponds to the value where a *step* is observed in the zero field-cooled hysteresis (Figure 2(a)). The field-cooled curves were measured by cooling the sample in magnetic field from room temperature to the measuring temperature and subsequently recording the magnetic hysteresis. For the sake of clarity only the part of the loop in the first quadrant is shown in the figure. It is clear that with the application of 25 kOe, the *steps* are smoothed out in the

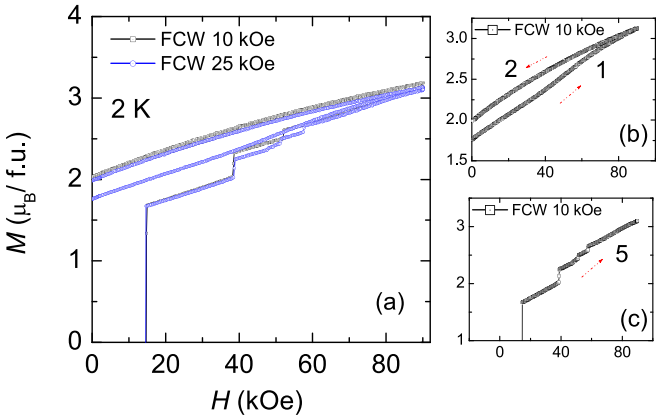

FIG. 3. The magnetic hysteresis at 2 K in field-cooled condition for two values of applied fields, 10 kOe and 25 kOe. With the application of the field, the *steps* are smoothed. (b) and (c) Enlarged views of the first quadrant of the hysteresis.

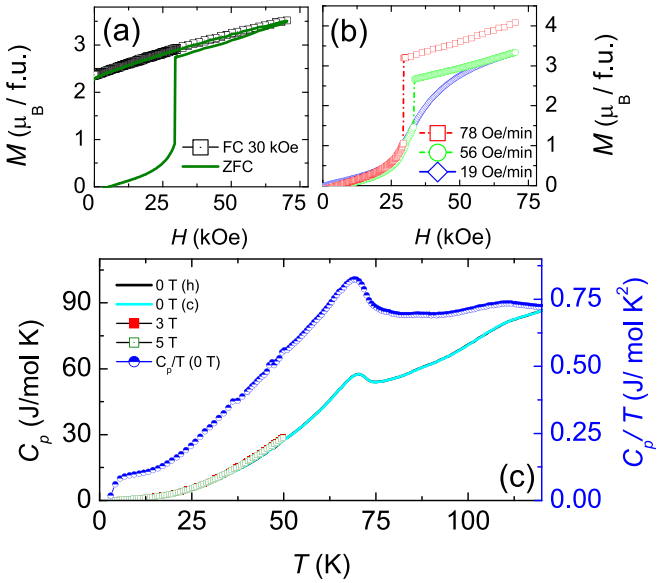

FIG. 4. (a) The *steps* disappear when the magnetic hysteresis is measured in field cooled protocol. (b) The sweep-rate of the applied field influences the *steps*. (c) The specific heat C_p of Y_2CoMnO_6 in applied fields of 0 T, 3 T, and 5 T. The C_p in zero field measured in heating (h) and cooling (c) cycles shows no evidence of a thermal hysteresis. C_p/T versus T for the 0 T data (black solid line) presents a "shoulder" near 8 K where the *steps* begin to appear in the magnetic hysteresis.

reverse sweep of the magnetic field. In the panels (b) and (c), enlarged sections of (a) are presented.

Figures 4(a) and 4(b) present the field-cooled hysteresis as well as the dependence of the *steps* on the sweep-rate of magnetic field at 3 K. The *steps* are absent in the field-cooled hysteresis where the value of the applied field for field-cooling is greater than ≈25 kOe. The *steps* depend on the sweep-rate of the magnetic field and from Figure 4(b) it can be seen that they disappear at slow sweep-rates. Below 8 K where the *steps* are present, the time-dependence of magnetic relaxation is flat suggesting that the *steps* do not originate from time-dependent magnetization dynamics, considering the sweep-rates used.

C. Specific heat

The specific heat C_p of Y_2CoMnO_6 in 0 T, 3 T, and 5 T are presented in Fig. 4(c). The magnetic phase transition at $T_c \approx 75$ K is reflected in the specific heat data as a broad anomaly. The specific heat was measured in heating (h) and cooling (c) cycles; however, no thermal hysteresis was observed. Magnetic fields up to 5 T do not perturb the specific heat anomaly. However, an anomaly is observed at ≈8 K when C_p/T versus T is plotted for 0 T as well as 5 T. The anomaly corresponds to the temperature below which the *steps* in magnetic hysteresis begin to appear.

From the magnetic measurements it is clear that Y_2CoMnO_6 displays effects of cationic disorder. The *steps* in magnetic hysteresis bear a close resemblance with martensitic-like transitions observed in many transition metal oxides and alloys systems. In order to obtain a clear handle of the defect content in the samples, we performed neutron diffraction experiments.

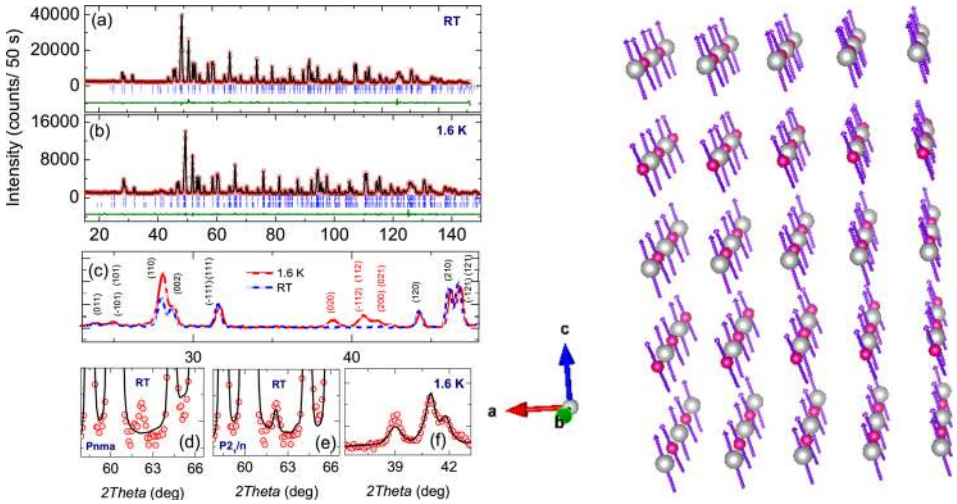

FIG. 5. (Left): The neutron powder diffraction patterns of Y_2CoMnO_6 obtained (a) at RT and (b) at 1.6 K are shown as red circles. A multi-phase model consisting of monoclinic structure with antisite disorder and orthorhombic phases was essential to obtain faithful Rietveld fits to the observed data. The magnetic structure was refined using a ferromagnetic model. (c) The diffraction patterns at the two temperatures with peaks indexed. Comparison of (d) and (e) makes it clear that some peaks were accounted for only in monoclinic symmetry. (f) The data at 1.6 K with an enlarged view of the magnetic peaks at $2\Theta \sim 39^\circ$ and the fits. (Right): The magnetic structure obtained from the analysis of 1.6 K-data. Pink and grey spheres differentiate Mn and Co atoms, respectively.

D. Neutron diffraction: Presence of antisite disorder

The crystal structure of $R_2MM'O_6$ double perovskite is commonly described either in monoclinic $P2_1/n$ or orthorhombic *Pnma* space groups, respectively, depending on whether it is perfectly ordered or disordered. In $P2_1/n$, the M/M' cations can occupy the Wyckoff positions 2*c* and 2*d* and hence this space group supports crystallographic ordering of cations. In the orthorhombic structure, the cations are distributed randomly at the 6*c* site and hence, disordered.

The neutron powder diffraction pattern of Y_2CoMnO_6 at room-temperature and at 1.6 K is presented in Figs. 5(a) and 5(b), respectively. The cationic order, mentioned above, is normally evident in the diffraction pattern as the **(011)** reflection.[12] In the case of Y_2CoMnO_6, the **(011)** reflection is weak suggesting that the degree of ordering is low. Rietveld refinements using ordered $P2_1/n$ or *Pnma* were not able to reproduce the experimental data faithfully. Hence, Rietveld refinements were performed for five models, *viz.*, (*i*) $P2_1/n(o)$, (*ii*) *Pnma*, (*iii*) $P2_1/n(o) + Pnma$, (*iv*) $P2_1/n(d)$, and (*v*) $P2_1/n(d) + Pnma$ assuming the presence of disorder. Here, $P2_1/n(o)$ is the ordered monoclinic phase and $P2_1/n(d)$ is the *antisite* disordered phase. The calculated profile for the $P2_1/n(o)$ model gave significant intensity for the **(011)** reflection at $2\Theta \approx 24^\circ$ which was not reproduced in the experimentally observed pattern. Moreover, from magnetization measurements, it was clear that a perfect ferromagnetic saturation moment was not attained even at 3 K, suggesting that disorder is present in the material. So, second, the *Pnma* model was checked. It was found that certain Bragg reflections, for example, at $2\Theta \approx 62^\circ$, were accommodated only in the monoclinic space group (see Figs. 5(d) and 5(e)). Consequently, a two-phase model incorporating both $P2_1/n$ and *Pnma* phases was introduced. Finite percentage of *antisite* disorder was introduced in the $P2_1/n$ phase. The best fit to the observed diffraction data was obtained for the model (*v*). The result of Rietveld refinement using this model is presented in Fig. 5 as black solid line. The reliability factor R_B for different models obtained after refinement are: $P2_1/n(o) = 4.37$, $Pnma = 17.7$, $(P2_1/n(o) + Pnma) = 4.34$, and $(P2_1/n(d) + Pnma) = 2.68$. From a quantitative analysis of the refinement results, it was found that Y_2CoMnO_6 consists of 62% of $P2_1/n(d)$ and 38% of *Pnma* phases, both of which are disordered phases which explains the weak **(011)** peak. The antisite occupancy in the monoclinic phase was estimated at nearly 70%.

Previous neutron diffraction study on La_2CoMnO_6 has shown that the Mn–O and Co–O bond distances do not change significantly between the *ordered* and *disordered* samples.[12] The Mn–O bond distances were found to be around 1.9 Å which compares fairly well with the reported bond distance for the Mn^{4+} ion, for example, in $CaMnO_3$.[31] The bond lengths and angles determined for Y_2CoMnO_6 at 300 K and 1.6 K are collected in Table I. The values of Mn–O and Co–O are comparable to the reported values for La_2CoMnO_6.[12] No significant variation in average bond distances at 300 K and 1.6 K are discernible. The refined structural parameters were used to calculate the bond valence sums (BVS) using the software called VaList.[32] The results of the BVS estimation are

TABLE I. The bond parameters of Y_2CoMnO_6 at room temperature and at 1.6 K. The bond distances are given in units of Å.

Bond parameter	300 K	1.6 K
Co–O1	2.049(9) × 2	2.033(10) × 2
Co–O2	2.155(9) × 2	2.182(11) × 2
Co–O3	2.096(9) × 2	2.088(9) × 2
$(Co\text{-}O)_{av}$	2.1	2.1
Mn–O1	1.854(9) × 2	1.864(10) × 2
Mn–O2	1.842(9) × 2	1.838(10) × 2
Mn–O3	1.916(10) × 2	1.892(9) × 2
$(Mn\text{-}O)_{av}$	1.87	1.86
⟨Co-O1-Mn⟩	146.7(4)°	146.7(4)°
⟨Co-O2-Mn⟩	147.0(4)°	144.5(4)°
⟨Co-O3-Mn⟩	148.4(4)°	148.4(4)°
⟨O-Mn/Co-O⟩	180°	180°

TABLE II. The BVS obtained for 300 K and 1.6 K data. The presence of multiple valence states for Co and Mn is clear.

Cation	Valence	BVS (RT)	BVS (1.6 K)
Co(2*c*)	+2	2.026(10)	2.014(1)
	+3	1.746(42)	1.736(42)
	+4	2.186(45)	2.172(46)
Co(2*d*)	+2	3.716(86)	3.768(88)
	+3	3.202(7)	3.248(8)
	+4	4.008(0)	4.066(0)
Mn(2*c*)	+2	2.642(32)	2.626(31)
	+3	2.434(19)	2.42(19)
	+4	2.370(41)	2.354(41)
Mn(2*d*)	+2	4.842(142)	4.912(146)
	+3	4.466(49)	4.53(51)
	+4	4.346(9)	4.408(10)

collected in Table II. Using the $P2_1/n(o)$ model lead to incorrect estimates of valences for the cations with significant standard deviations. Only in the case of model (v) did we obtain reliable values for the valence states. It was observed that though the predominant valence states of Co and Mn are +2 and +4, respectively, other valences of Co and Mn in the form of $(Co/Mn)^{2+}$ and $(Co/Mn)^{3+}$ are also present in the sample as a result of *antisite* disorder. The BVS estimates support the scenario of *antisite* disorder that emerged from magnetometry and structural refinement.

The high disorder in the present set of samples could directly result from the preparative methods itself. High-temperature solid state synthesis of double perovskites usually results in samples with significant antisite disorder. Specific synthesis routes with controlled heating and cooling rates which control the kinetics of the reaction are essential to obtain samples with high degree of cationic order.[12,33] The polycrystalline samples used in the present study were prepared by fast rates of firing and cooling at elevated temperatures and hence resulted in higher content of disorder.

In Figure 5(c), selected regions of the refinement pattern at room temperature and 1.6 K are plotted together with indexed Bragg peaks. At 1.6 K the magnetic peaks appear as **(020)**, **(112)**, **(021)** reflections and enhancement of intensity for the **(110)** peak is evident. The nuclear structure at 1.6 K was refined using the same multi-phase model employed for the room temperature case which showed that the majority phase at 1.6 K is $P2_1/n(d)$. The diffraction data indicate predominantly ferromagnetic order with most of the magnetic peaks occurring at the same position as the nuclear Bragg peaks.

In order to solve the magnetic structure, representational analysis was employed using the software SARAh[30] by inputting the nuclear phase $P2_1/n$ in which the Co and Mn occupy the Wyckoff positions 2*c* ($\frac{1}{2}$, 0, 0) and 2*d* (0, $\frac{1}{2}$, 0). The magnetic representation, Γ in terms of irreducible representations Γ_k for these sites is written as, $\Gamma_{mag} = 3\Gamma_1^1 + 0\Gamma_2^1 + 3\Gamma_3^1 + 0\Gamma_4^1$. The model-fit to the observed neutron data at 1.6 K is presented as a black solid line in Fig. 5(b). While both the magnetic models were tested, Γ_3 offered a better fit to the observed data with a low R_{mag}. The magnetic moments were initially constrained parallel to crystallographic axes but that did not yield a good fit to the observed data and hence non-zero components along all the three axes were assumed. Moreover, magnetic intensity for the **(002)** reflection is suggestive of the fact that the magnetic moments cannot be parallel to the *c* axis.[34] The magnetic structure that resulted from the refinement strategy for 1.6 K is presented in the inset of Fig. 5(b). Similar to the case of Nd_2CoMnO_6, broad and asymmetric peak at $2\theta \sim 38^\circ$ was observed, which was well reproduced by assuming magnetic moment components along all the three axes and indexed as **(020)** reflection in $P2_1/n$, Fig. 5(f). The value of average magnetic moment at 1.6 K as extracted from the refinement is $M_{Co/Mn} = 1.73\ \mu_B$/f.u. The antisite disorder in the sample and possible presence of Co^{2+} in divalent low-spin state which do not take part in magnetic exchange can contribute to the observed reduction in the magnetic moment value. The atomic positions, lattice parameters and the quality measures of different structural phases after refinement at room temperature and at 1.6 K are collected in Table III.

IV. ORIGIN OF THE "STEPS"

The *steps* in magnetic hysteresis observed in Y_2CoMnO_6 are qualitatively similar to those observed in intermetallics[21,35] or phase segregated manganites.[23,36] In the case of

TABLE III. Lattice parameters, atomic positions, phase fraction, and magnetic moments of Y_2CoMnO_6 obtained after Rietveld refinement of the neutron diffraction data at room-temperature and 1.6 K. The refinement was carried out using a two-phase model with $P2_1/n$ and *Pnma* where antisite disorder was also incorporated. The Co and Mn cations occupy the 2*c* ($0\ \frac{1}{2}\ 0$) and 2*d* ($\frac{1}{2}\ 0\ 0$) Wyckoff positions, respectively, in $P2_1/n$ while 6*c* in *Pnma*.

	$T = 300$ K		$T = 1.6$ K	
	$P2_1/n$	*Pnma*	$P2_1/n$	*Pnma*
a (Å)	5.2407(3)	5.6007(2)	5.2352(1)	5.5989(1)
b (Å)	5.5952(6)	7.4795(1)	5.5919(2)	7.4666(1)
c (Å)	7.4808(2)	5.2404(2)	7.4686(3)	5.2341(1)
β (°)	89.7601(45)	90	89.8083(40)	90
Y *x*	0.9801(15)	0.0728(5)	0.9757 (12)	0.0755(4)
y	0.0763(15)	0.25	0.0695(12)	0.25
z	0.2466(10)	−0.075(5)	0.2469(10)	−0.0173(9)
O(1) *x*	0.0998(18)	0.4633(7)	0.0995(21)	0.4616(6)
y	0.4661(20)	0.25	0.4659(23)	0.25
z	0.2632(11)	0.1084(6)	0.2616(14)	0.1075(6)
O(2) *x*	0.7116(16)	0.3041(5)	0.7072(17)	0.3039(5)
y	0.3239(19)	0.0540(3)	0.3322(21)	0.0558(3)
z	0.4514(13)	0.6901(5)	0.4496(15)	0.6912(5)
O(3) *x*	0.6804(16)		0.6774(16)	
y	0.2892(17)		0.2884(17)	
z	0.0524(13)		0.0449(14)	
M_{av} (Co)			1.37 μ_B/f.u.	
M_{av} (Mn)			0.79 μ_B/f.u.	
R_p	…	6.47	…	6.24
R_{wp}	…	7.24	…	7.29
R_B	2.68	2.04	1.32	1.49
R_{mag}			2.88	
χ^2	…	5.67	…	2.16
Phase fraction	62.02(2.56)%	37.98(1.04)%	72.00(1.82)%	28.00(0.50)%

phase separated manganites, the steps were attributed to the intrinsic thermodynamic property of the charge ordered phase.[23] However, non-charge ordered manganites also displayed such *step*-like features[37] thus, making it clear that charge-order may not be a necessary condition for the occurrence of *steps*. Multi-step magnetization behaviour is often observed in pure antiferromagnets where multiple magnetic arrangements between the final antiferromagnetic and the paramagnetic phases are possible.[38] It can occur in site-diluted antiferromagnets where random distribution of magnetic vacancies can lead to spin-reversals within the clusters of magnetic vacancies. These scenarios require that unique, reproducible critical fields be present in the system. However, in Y_2CoMnO_6, the modification of the steps observed under different field-sweep rates and field-cooling conditions point to the fact that there are no unique critical fields. This implies that the *steps* in the present case cannot be explained on the basis of spin reversals or multiple magnetic arrangements. Since no features of a spin-glass ground state is reproduced in ac susceptibility experiments (not presented), the role of spin freezing is also ruled out.

Martensitic-like transformations in which low field antiferromagnetic state transforms to ferromagnetic state through strong magneto-structural coupling offered a fitting explanation in the case of intermetallics.[21] The applied magnetic field results in lattice distortion in the compound and due to the difference in crystallographic structures between the low-field and high-field phases, elastic strain develops at the interface between the ferromagnetic and antiferromagnetic phases. In the presence of applied field, the ferromagnetic phase tends to grow at the expense of the antiferromagnetic phase by overcoming the resistance at the interface. An analogous explanation based on *antisite* disorder and the antiphase boundaries can be put forward in the present case of Y_2CoMnO_6.

The structural analysis, using neutron powder diffraction has made it clear that there is significant antisite disorder in this material. In Fig. 6(a), the diffraction patterns recorded at various temperatures are presented. Note that a weak reflection at $2\Theta \approx 22^\circ$ which cannot be indexed in the monoclinic or orthorhombic structure appears in the patterns recorded at temperatures below the T_c. This reflection suggests antiferromagnetic interactions present in the material which arises due to antisite disorder.[5] Hence, a scenario of magnetic domains with mixed interactions separated by antiphase boundaries could be apt to describe the magnetic nature of Y_2CoMnO_6.

In order to give a semi-quantitative description, we employ a model that has been recently developed for the phase separated manganites[39] where the thermally activated motions of pinned ferromagnetic and antiferromagnetic interfaces are assumed. Borrowing the same framework, we use the relation, $\chi = (\frac{3M_0}{H_c})(\frac{\delta D_c}{D})$, where $\chi \sim (\frac{\partial M}{\partial H})$, M_0 is the spontaneous magnetization proportional to the ferromagnetic fraction, H_c is the critical field, and δD_c denotes the increment in the size of the ferromagnetic cluster of size D. According to the relation, a scaling plot of χ versus $(\frac{3M_0}{H_c})$ should give a straight line, which is shown in Fig. 6(b) for Y_2CoMnO_6. The domain structure that results from the

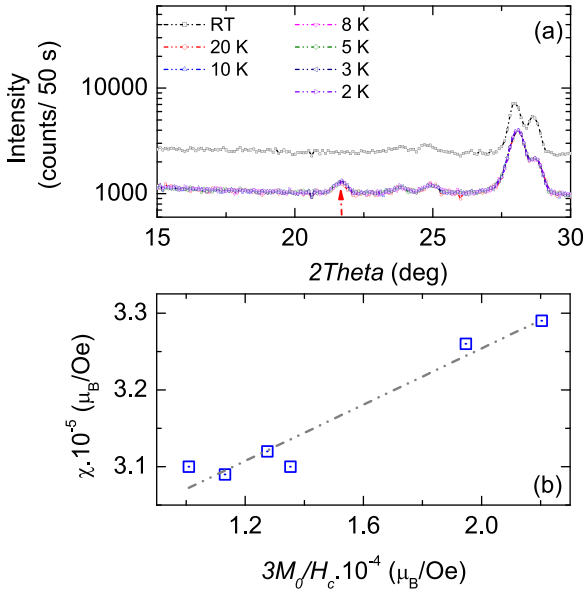

FIG. 6. (a) The powder diffraction patterns at different temperatures show that a weak reflection emerges at $2\Theta \approx 22^\circ$ (marked by a red arrow) which is not indexed in the monoclinic structure. This peak suggests the presence of antiferromagnetic interactions due to antisite disorder. The room temperature data is shown off-set from the rest. (b) Magnetic susceptibility, χ, of Y_2CoMnO_6 as a function of the scaling parameter $3M_0/H_c$ where M_0 is the spontaneous magnetization and H_c is the critical field. A more-or-less linear behaviour is observed which supports the scenario of sudden growth of ferromagnetic fractions upon the application of external magnetic field.

antisite disordered regions consists of predominantly ferromagnetic regions with antiferromagnetic antiphase boundaries.[40] Application of external magnetic field leads to the sudden growth of the ferromagnetic regions which leads to the *steps* in magnetic hysteresis (see Fig. 7). The modification of the *steps* under different field-sweep rates can also be linked to such a scenario. Strong pinning of the magnetic domains at the antiphase boundaries have been experimentally observed in Ba_2FeMoO_6.[17] The magnetic domain structure is significantly affected by the crystallographic antiphase boundary and the application of external magnetic field changes the domain structure further.

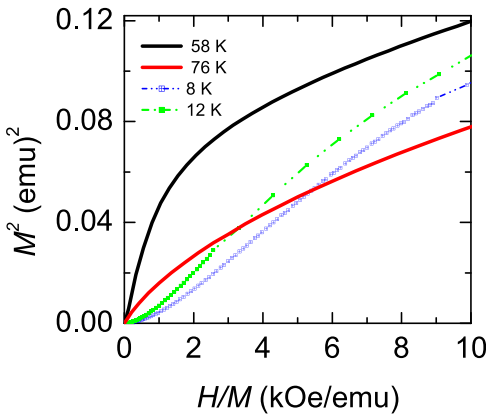

FIG. 7. The Arrott's plots derived from the magnetic hysteresis data of Y_2CoMnO_6 near the paramagnetic to ferromagnetic transition at $T_c \sim 75$ K and also at low temperature just close to the *step*-like features. From the nature of the slope of the curves, it is clear that the low temperature curves exhibit first-order-like character.

V. CONCLUSIONS

The important role played by *antisite* disorder in the magnetic properties of rare earth double perovskites is brought out through detailed magnetometry and neutron diffraction studies on Y_2CoMnO_6. The content of disorder in this compound is quantified through diffraction experiments. It is found that Y_2CoMnO_6 consists of a mixed phase of $P2_1/n$ and *Pnma* structures with nearly 70% *antisite* disorder. The disorder effects are also supported by the bond valence sums estimation. The sharp *steps* in magnetic hysteresis originate from the antisite disordered ferromagnetic domains separated by antiferromagnetic antiphase boundaries. The *steps* are influenced by the magnitude of the applied magnetic field as well as the sweep-rate. In the light of multiferroicity being proposed and observed in rare earth double perovskites, it is important to incorporate the *antisite* disorder to obtain a realistic explanation of the observed physical properties.

[1]N. S. Rogado, J. Li, A. W. Sleight, and M. A. Subramanian, Adv. Mater. **17**, 2225 (2005).
[2]D. J. Singh and C. H. Park, Phys. Rev. Lett. **100**, 087601 (2008).
[3]K.-I. Kobayashi, T. Kimura, H. Sawada, K. Terakura, and Y. Tokura, Nature **395**, 677 (1998).
[4]S. Y. Vilar, E. D. Mun, V. S. Zapf, B. G. Ueland, J. S. Gardner, J. D. Thompson, J. Singleton, M. Sánchez-Andújar, J. Mira, N. Biskup, M. A. S. Rodríguez, and C. D. Batista, Phys. Rev. B **84**, 134427 (2011).
[5]G. Sharma, J. Saha, S. D. Kaushik, V. Siruguri, and S. Patnaik, Appl. Phys. Lett. **103**, 012903 (2013).
[6]S. Kumar, G. Giovannetti, J. van den Brink, and S. Picozzi, Phys. Rev. B **82**, 134429 (2010).
[7]M. Ležaić and N. A. Spaldin, Phys. Rev. B **83**, 024410 (2011).
[8]H. Das, U. V. Waghmare, T. Saha-Dasgupta, and D. D. Sarma, Phys. Rev. Lett. **100**, 186402 (2008).
[9]S. Lv, X. Liu, H. Li, L. Han, Z. Wang, and J. Meng, J. Comput. Chem. **33**, 1433 (2012).
[10]J. B. Goodenough, Phys. Rev. **100**, 564 (1955).
[11]J. Kanamori, J. Phys. Chem. Solids **10**, 87 (1959).
[12]A. J. Barón-González, C. Frontera, J. L. García-Muñoz, B. Rivas-Murias, and J. Blasco, J. Phys.: Condens. Matter **23**, 496003 (2011).
[13]R. I. Dass and J. B. Goodenough, Phys. Rev. B **67**, 014401 (2003).
[14]R. I. Dass, J. Q. Yan, and J. B. Goodenough, Phys. Rev. B **68**, 064415 (2003).
[15]J. M. Greneche, M. Venkatesan, R. Suryanarayanan, and J. M. D. Coey, Phys. Rev. B **63**, 174403 (2001).
[16]T. Fang, Phys. Rev. B **71**, 064401 (2005).
[17]T. Asaka, X. Z. Yu, Y. Tomioka, Y. Kaneko, T. Nagai, K. Kimoto, K. Ishizuka, Y. Tokura, and Y. Matsui, Phys. Rev. B **75**, 184440 (2007).
[18]M. S. Senn, S. A. J. Kimber, A. M. A. Lopez, A. H. Hill, and J. P. Attfield, Phys. Rev. B **87**, 134402 (2013).
[19]J. R. Friedman, M. P. Sarachik, J. Tejada, and R. Ziolo, Phys. Rev. Lett. **76**, 3830 (1996).
[20]V. Hardy, M. R. Lees, O. A. Petrenko, D. M. Paul, D. Flahaut, S. Hébert, and A. Maignan, Phys. Rev. B **70**, 064424 (2004).
[21]B. Maji, K. G. Suresh, and A. K. Nigam, Europhys. Lett. **91**, 37007 (2010).
[22]S. N. Jammalamadaka, N. Mohapatra, S. D. Das, K. K. Iyer, and E. V. Sampathkumaran, J. Phys.: Condens. Matter **20**, 425204 (2008).
[23]R. Mahendiran, A. Maignan, S. Hébert, C. Martin, M. Hervieu, B. Raveau, J. F. Mitchell, and P. Schiffer, Phys. Rev. Lett. **89**, 286602 (2002).
[24]S. B. Roy, M. K. Chattopadhyay, P. Chaddah, and A. K. Nigam, Phys. Rev. B **71**, 174413 (2005).
[25]A. Haldar, K. G. Suresh, and A. K. Nigam, Phys. Rev. B **78**, 144429 (2008).
[26]T. Chatterji, B. Frick, and H. S. Nair, J. Phys.: Condens. Matter **24**, 266005 (2012).
[27]V. F. Sears, Neutron News **3**, 29 (1992).
[28]H. M. Rietveld, J. Appl. Cryst. **2**, 65 (1969).
[29]J. Rodriguez-Carvajal, Physica B **192**, 55 (1993).
[30]A. S. Wills, Physica B **276**, 680 (2000).
[31]E. S. Božin, A. Sartbaeva, H. Zheng, S. A. Wells, J. F. Mitchell, T. Proffen, M. F. Thorpe, and S. J. L. Billinge, J. Phys. Chem. Solids **69**, 2146 (2008).
[32]A. S. Wills, "VaList," Department of Chemistry, University College London, 2010.
[33]T. Shimada, J. Nakamura, T. Motohashi, H. Yamauchi, and M. Karppinen, Chem. Mater. **15**, 4494 (2003).
[34]I. O. Troyanchuk, D. D. Khalyavin, J. W. Lynn, R. W. Erwin, Q. Huang, H. Szymczak, R. Szymczak, and M. Baran, J. Appl. Phys. **88**, 360 (2000).
[35]E. M. Levin, V. K. Pecharsky, K. A. Gschneidner, Jr., and G. J. Miller, Phys. Rev. B **64**, 235103 (2001).
[36]V. Hardy, S. Majumdar, M. R. Lees, D. Mck. Paul, C. Yaicle, and M. Hervieu, Phys. Rev. B **70**, 104423 (2004).
[37]V. Hardy, S. Hébert, A. Maignan, C. Martin, M. Hervieu, and B. Raveau, J. Magn. Magn. Mater. **264**, 183 (2003).
[38]E. Stryjewski and N. Giordano, Adv. Phys. **26**, 487 (1977).
[39]D. Niebieskikwiat and R. D. Sánchez, J. Phys.: Condens. Matter **24**, 436001 (2012).
[40]C. Meneghini, S. Ray, F. Liscio, F. Bardelli, S. Mobilio, and D. D. Sarma, Phys. Rev. Lett. **103**, 046403 (2009).